

Two-Electron Correlations in the Metallic Electron Gas

Zhiyi Li^{1,2,*}, Pengcheng Hou^{2,*}, Bao-Zong Wang^{3,†}, Youjin Deng^{1,2,4,‡} and Kun Chen^{5§}

¹ Department of Modern Physics, University of Science and Technology of China, Hefei, Anhui 230026, China

² Hefei National Laboratory, University of Science and Technology of China, Hefei 230088, China

³ International Center for Quantum Materials, School of Physics, Peking University, Beijing 100871, China

⁴ Hefei National Research Center for Physical Sciences at the Microscale and School of Physical Sciences, University of Science and Technology of China, Hefei 230026, China and

⁵ CAS Key Laboratory of Theoretical Physics, Institute of Theoretical Physics, Chinese Academy of Sciences, Beijing 100190, China

We present high-precision *ab initio* calculations of the four-point vertex function for the three-dimensional uniform electron gas using variational diagrammatic Monte Carlo. From these results, we extract Landau parameters that demonstrate a density-driven crossover from underscreening to overscreening. Guided by our numerical data, we propose a charge-based Kukkonen–Overhauser effective interaction within the local-density approximation, supplemented by a small s-wave correction (sKO⁺), which accurately captures the electron–electron scattering amplitude. Using our numerically determined scattering amplitude, together with the sKO⁺ ansatz, we compute the electron-electron contribution to the thermal resistivity, demonstrating excellent agreement with experimental measurements in simple metals.

Introduction.— The collective behavior of interacting electrons gives rise to some of the most profound and challenging problems in condensed matter physics [1], including high-temperature superconductivity [2], strange metallicity [3], and the emergence of topological phases [4]. The uniform electron gas (UEG)—an idealized model of electrons moving in a uniform neutralizing background—provides the quintessential canvas for understanding correlations originating solely from the Coulomb interaction [5]. While the single-particle properties of this system have been extensively studied [6], a comprehensive understanding of two-electron correlations has remained elusive despite their fundamental importance.

The key to this problem lies in the four-point vertex function, which is central to understanding Fermi liquid behavior [7, 8], pairing instabilities [9], and electron-electron scattering rates that govern transport phenomena [10]. A first-principles determination has historically been impeded by its complex dependence on multiple momentum and frequency variables. The immense computational cost associated with this high dimensionality poses a severe challenge, forcing many theoretical frameworks to rely on approximations, such as low-order truncations in diagrammatic methods or the local approximations in dynamical mean-field extensions and post-GW schemes [11–14]. At the same time, conventional quantum Monte Carlo techniques also face challenges, as the vertex function captures subtle many-body correlations that are difficult to extract directly from the static ground-state densities typically sampled in these simulations. This theoretical gap is particularly pressing today, as advances in two-electron photoemission and multidimensional electronic spectroscopies begin to access many-electron correlations experimentally [15–17].

The consequences of this theoretical gap are partic-

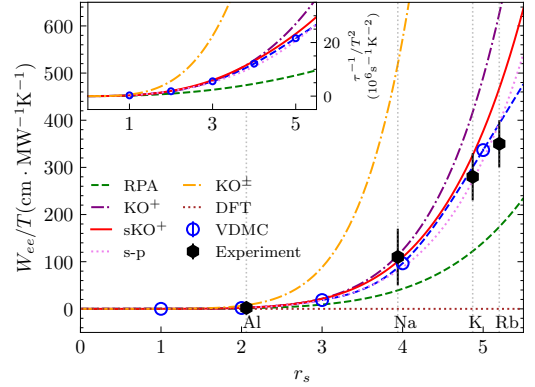


FIG. 1. The electron-electron contribution to the thermal resistivity W_{ee} as a function of density parameter r_s in the metallic regime derived through our numerical results (blue circles) through the variational diagrammatic Monte Carlo (VDMC) method and some theoretical models as the random phase approximation (RPA), s-p approximation [18, 19], the original Kukkonen-Overhauser interaction [20] (KO^\pm) and the one with charge channel only (KO^+). For comparison, we plot the experimental data (black circle) for some simple metals [21–24]. The solid red line presents our proposed sKO⁺ model, the KO^+ model with s-wave corrections, which shows good agreement with the VDMC results and the experimental measurements. The inset shows the results of the electron-electron scattering rate.

ularly stark in the study of transport phenomena, presenting a long-standing challenge to the first-principles description of thermal conductivity in simple metals. Here, e-e scattering is understood to be a primary contributor to the experimentally observed deviations from the Wiedemann–Franz law [21–26], an effect that conventional density functional theory (DFT) struggles to account for [27]. Previous attempts to resolve this issue using many-body theories, such as the random

phase approximation (RPA) [28, 29] and the Kukkonen-Overhauser (KO) interaction [20, 29], have also resulted in thermal resistivity values that disagree with experimental measurements. Consequently, finding a theoretical ansatz for the effective electron-electron interaction that yields precise quantitative agreement with experiment remains an open challenge.

In this work, we address this challenge using the variational diagrammatic Monte Carlo (VDMC) method [30–33], which combines a variational principle with high-order, controlled stochastic summation of Feynman diagrams [34–44]. For the 3D UEG, we compute the four-point vertex up to sixth order, comprehensively characterizing two-electron correlations and extracting the Landau parameters $F_{0,1,2}^{s,a}$. This provides a long-sought, first-principles quantitative determination of these key Fermi-liquid parameters. Our results reveal a crossover from underscreening to overscreening [45–47], where collective screening drives the static dielectric function negative, effectively inverting the test-charge interaction from repulsive to attractive. This transition is characterized by the Landau parameter F_0^s approaching -1 , signaling a divergence in electronic compressibility and the onset of a strongly correlated regime.

Furthermore, we calculate the full e-e scattering amplitude with high precision across the entire Fermi surface. Crucially, these results serve as the foundation for our proposal of a robust effective interaction: a charge-based KO model within the local density approximation (LDA), supplemented by an s-wave correction (sKO⁺). This ansatz effectively resolves the discrepancies found in widely used approximations, such as the RPA and the KO interaction. Notably, our sKO⁺ ansatz offers a consistent description of electron correlations across all energy scales, extending the high precision rigorously established on the Fermi surface.

Crucially, our first-principles results for the e-e scattering amplitude enable a direct calculation of the thermal resistivity, resolving the long-standing discrepancy between previous theoretical approximations and experimental measurements. As shown in Fig. 1, the resistivity derived from our calculated scattering amplitude is in good agreement with experimental data [21–24]. Moreover, the thermal resistivity calculated using our proposed sKO⁺ model also closely matches the experimental values, confirming the validity of our comprehensive approach.

Methods.— We employ the VDMC framework [30–40], which combines a robust variational principle with stochastic sampling of Feynman diagrams. This approach enables controlled evaluation of high-order perturbative contributions to the four-point vertex function of the uniform electron gas.

The central idea is to reorganize many-body perturbation theory around a variationally optimized screened interaction. Counterterms are introduced to preserve the

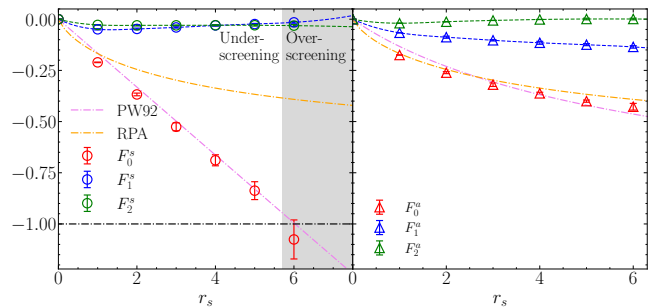


FIG. 2. Numerical results of the symmetric (left panel) and antisymmetric (right panel) Landau parameters versus r_s , which confirms the rapid convergence of the Legendre expansion. The linear decrease of F_0^s with r_s , which approaches -1 at $r_s^c \approx 5.7$, reveals the crossover of the Coulomb screening effect from underscreening to overscreening [45]. For comparison, the orange dash-dot line shows the F_0 calculated from the RPA vertex. The violet dash-dot line presents the dimensionless static exchange-correlation (XC) kernel $f_{\text{XC}}(q=0)N_F$ for the uniform electron gas derived from the PW92 energy functional [48], which demonstrates the approximate equality of the XC kernel and the zeroth Landau parameter. The corresponding numerical data are listed in Table S1 of the Supplemental Material.

exact physics of the original Hamiltonian, ensuring that the expansion remains unbiased. The diagrammatic series is then sampled as a computational graph, where counterterm contributions are obtained through Taylor-mode automatic differentiation.

Our implementation incorporates automated high-order renormalization and GPU-accelerated integration routines [41], allowing efficient evaluation of high-dimensional diagrams up to sixth order. This combination provides unprecedented computational reach for effective field theories in strongly interacting systems.

A key feature of VDMC is the presence of systematic cancellations between competing diagrams, which accelerates convergence of physical observables. For quantities such as the Landau parameters, this leads to remarkably stable results: for instance, at $r_s = 4$ the combined parameters converge by sixth order, with uncertainties estimated from the spread of the last three expansion orders which is shown in Fig. S1 in the supplemental material.

Results.— The 3D UEG is modeled by the reduced temperature $\Theta = T/T_F$ and the density parameter, the Wigner-Seitz radii $r_s = (\frac{3}{4\pi n})^{1/3}$ with Coulomb interaction $v_q = 4\pi e^2/q^2$, where T_F is the Fermi temperature, n is the electron density. We investigate the parameter regimes defined by $\Theta = 0.025$ and 0.05 , with r_s ranging from 1 to 6. Within Landau-Silin theory [49, 50], the effective short-range interaction between quasiparticles on the Fermi surface $f_{\sigma\sigma'}(\theta)$, which encapsulates many-body correlations, is obtained from the small-frequency and long-wavelength limit of the four-point vertex dia-

gram Γ_4 as

$$f_{\sigma\sigma'}(\theta) = z^2 \lim_{\mathbf{q} \rightarrow 0} [\Gamma_4^{\sigma\sigma'}(\mathbf{k}_1\omega_{-1}, \mathbf{k}_2\omega_0; \mathbf{k}_1 + \mathbf{q}\omega_0) - v_q]. \quad (1)$$

Here, θ is the angle between the incoming momentum \mathbf{k}_1 and \mathbf{k}_2 on the Fermi surface, $\omega_0 = i\pi T$, $\omega_{-1} = -i\pi T$ are the Fermionic Matsubara frequency and z is the quasiparticle renormalization factor derived from the calculation of self-energy [41]. Meanwhile, the two-electron scattering amplitude, $a_{\sigma\sigma'}(\theta, \phi)$, is related to the four-point vertex for elastic scattering of quasiparticles on the Fermi shell as:

$$a_{\sigma\sigma'}(\theta, \phi) = z^2 \Gamma_4^{\sigma\sigma'}(\mathbf{k}_1\omega_0, \mathbf{k}_2\omega_0; \mathbf{k}_3\omega_0), \quad (2)$$

where ϕ is the angle between the plane defined by $(\mathbf{k}_1, \mathbf{k}_2)$ and the plane defined by the outgoing momenta $(\mathbf{k}_3, \mathbf{k}_4)$.

Figure 2 shows the dimensionless spin-symmetric and antisymmetric Landau parameters $F_l^{s,a}$ ($l = 0, 1, 2$) as functions of r_s . These parameters, which characterize fundamental many-body interactions in the electron gas, are defined as Legendre components of the dimensionless quasiparticle interaction $F^{s,a}(\theta) = (F_{\uparrow\uparrow}(\theta) \pm F_{\uparrow\downarrow}(\theta))/2$ with $F_{\sigma\sigma'}(\theta) = N_F^* f_{\sigma\sigma'}(\theta)$, where $N_F^* = \frac{m^*}{m} N_F$ is the renormalized density of states at the Fermi surface.

One pivotal observation is the linear decrease of the compressibility-related parameter: $F_0^s \approx -0.17r_s$. This behavior drives the Coulomb screening effect from “underscreening” to “overscreening”, with the crossover occurring at $F_0^s = -1$ where the proper compressibility approaches zero and the ion-ion interaction becomes effectively attractive at large distances [46, 51]. Our calculations show this crossover occurs near $r_s^c \approx 5.7$, which is close to the previous theoretical predictions in Ref. [45] of $r_s = 5.25$ [52]. Importantly, the higher-order Landau parameters remain significantly smaller than F_0^s , demonstrating the rapid convergence of the Legendre expansion. For comparison, Fig. 2 also shows F_0^s obtained from the RPA vertex and the dimensionless zero-momentum static XC kernel $f_{\text{XC}}^\pm(q=0)N_F$ derived from the PW92 energy functional [48]. The PW92 XC kernels agree well with our numerically extracted $F_0^{s,a}$, confirming the approximate equality between the static zero-transfer-momentum XC kernel and the corresponding Landau parameters as

$$f_{\text{XC}}^\pm(q=0)N_F \approx F_0^{s,a}, \quad (3)$$

for r_s in the metallic regime—an relation specific to the homogeneous electron liquid, and not generally shared by arbitrary Fermi liquids. The theoretical insights of this relation will be discussed in Sec. III in the supplemental material.

Besides, the parameter F_1^s plays a crucial role in determining the effective mass m^* through the relation $m^*/m = 1 + F_1^s$, where m represents the bare electron mass. Our finding that F_1^s approaches zero in the metallic density regime, which confirms the findings through

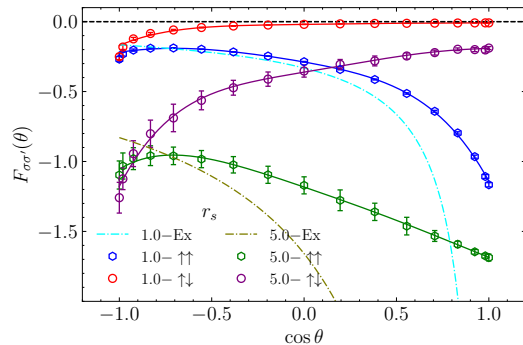


FIG. 3. Angle-resolved Landau quasiparticle interaction for $r_s = 1, 5$ with parallel and antiparallel spin. The dotted-dashed line represents the bare exchange Coulomb interaction. The larger deviation from the bare interaction for $r_s = 5$ indicates the Coulomb screening increases as the electron density decreases.

the variational Monte Carlo and VDMC [31, 53, 54] that the effective mass approximately equals the bare mass in this regime.

Figure 3 displays the angle-resolved Landau quasiparticle interaction $F_{\sigma\sigma'}(\theta)$ versus $\cos \theta$ at $r_s = 1$ and 5 for both parallel ($\uparrow\uparrow$) and anti-parallel spin ($\uparrow\downarrow$) configurations. The bare exchange Coulomb interaction $W_{\text{Ex}}(\mathbf{k}_1, \mathbf{k}_2) = -N_F v(|\mathbf{k}_1 - \mathbf{k}_2|)$ is shown for comparison. In the parallel spin channel, many-body screening substantially modifies the quasiparticle interaction from the bare exchange. At $r_s = 1$, $F_{\uparrow\uparrow}(\theta)$ deviates from the bare exchange primarily at small angles with rapid variation as $\theta \rightarrow \pi$, while at $r_s = 5$, deviations occur across all angles with a smoother angular dependence. This evolution indicates increasing locality of the quasiparticle interaction and enhanced screening at larger r_s values. For the anti-parallel spin channel, where the bare two-electron short-range interaction vanishes, the quasiparticle interaction emerges entirely from many-body effects. Notably, $F_{\uparrow\downarrow}(\theta)$ exhibits minima at $\theta = \pi$ for both r_s values, where the incoming electron’s momentum and spin are opposite, potentially relating to Cooper pairing instability from dynamic screening potential effects [55].

Figure 4 presents the dimensionless two-electron scattering amplitude, $A^{\sigma\sigma'}(\theta, \phi) = N_F^* a_{\sigma\sigma'}(\theta, \phi)$, for the uniform electron gas. We analyse the forward-scattering ($\phi = 0$) and Cooper ($\theta = \pi$) channels at $r_s = 1$ and 5 for $T/T_F = 0.025$, and include $T/T_F = 0.05$ for $r_s = 5$. Comparison of these datasets demonstrates that our results have reached the zero-temperature limit within error bars, except for the Cooper channel divergence caused by the Tolmachev singularity [55]. Crucially, as this singularity is confined to a phase space of measure zero, it has a negligible impact on Fermi-surface integrals in general. Based on our numerical results, we conjecture an effective interaction (sKO⁺), which is more accurate than the common effective interaction, for example, the RPA and

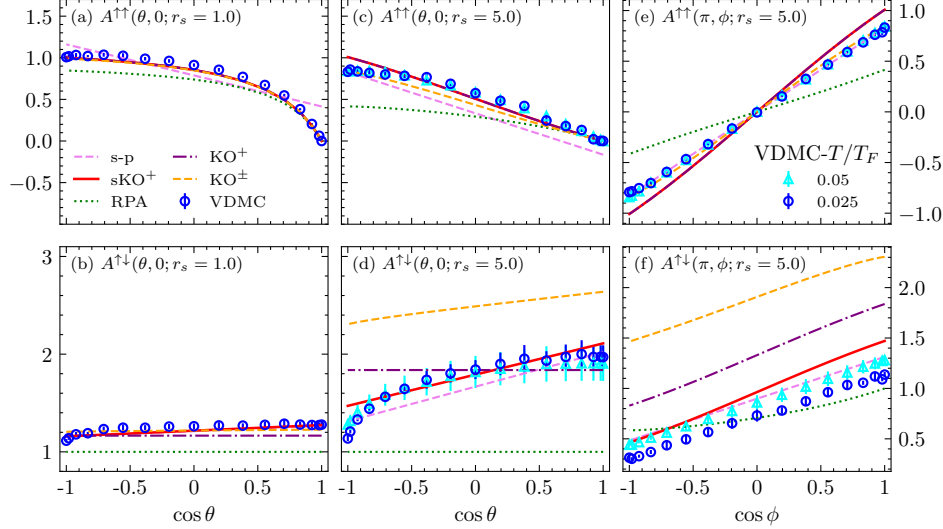


FIG. 4. The dimensionless two-electron scattering amplitude $A^{\sigma\sigma'}(\theta, \phi)$ for parallel ($\uparrow\uparrow$, top row) and anti-parallel ($\uparrow\downarrow$, bottom row) spins at $r_s = 1$ and $r_s = 5$ at $T/T_F = 0.025$. Panels (a-d) show the forward scattering channel ($\phi = 0$). Panels (e-f) show the Cooper channel ($\theta = \pi$). Our VDMC results (symbols) are compared against several theoretical models. We also plot the $s\text{KO}^+$ conjectured through analyzing the deviation of our VDMC results and the KO^+ interaction, which shows good agreement with the numerical results. For $r_s = 5$, numerical results at $T/T_F = 0.05$ are also plotted. The divergence of the scattering amplitude at the two effectively low temperature in the Cooper channel is consistent with the expected logarithmic divergence of the four-point vertex function as $T \rightarrow 0$ [55].

KO. This ansatz is based on the charge KO interaction within the LDA, $f_{\text{XC}}^+(q) \approx f_{\text{XC}}^+(0) (= f_{\text{XC}}^+ \text{ below})$, supplemented by an s-wave correction δR for the antiparallel spin configuration:

$$R_{\mathbf{k}_1\mathbf{k}_2\mathbf{q}}^{\sigma\sigma'} = \frac{v_q + f_{\text{XC}}^+}{1 - [v_q + f_{\text{XC}}^+(0)]\Pi_0(q)} - f_{\text{XC}}^+ + \delta R^{\sigma\sigma'} \quad (4)$$

$$\delta R_{\mathbf{k}_1\mathbf{k}_2\mathbf{q}}^{\sigma\sigma'} = (1 - \delta_{\sigma\sigma'}) \left[C_0 + C_2 \frac{(\mathbf{k}_1 - \mathbf{k}_2)^2 + (\mathbf{k}_1 - \mathbf{k}_2 - 2\mathbf{q})^2}{2} \right]. \quad (5)$$

The form of this correction term δR is derived from a detailed residual analysis. We performed a polynomial expansion on the residual difference between our numerical data and the KO^+ ansatz (see Sec V in the supplemental Material), which indicates that such corrections are necessary only for the antiparallel spin channel. Consequently, we formulate δR using an ansatz inspired by effective field theory for dilute Fermi gases [56, 57], identifying the expansion coefficients C_0 and C_2 as the s-wave scattering length and effective range. With this correction, the $s\text{KO}^+$ ansatz effectively describes the full electron-electron scattering amplitude across all tested densities and channels as shown in Fig. 4.

To highlight the advantages of the proposed $s\text{KO}^+$ ansatz, we also benchmark common theoretical models against our high-precision VDMC data in Fig. 4, revealing the significant inadequacies of standard approximations. (i) RPA: The simplest case of Eq. (4) where $f_{\text{XC}}^+(0) = 0$ and $\delta R = 0$ —is clearly inadequate, espe-

cially in the low-density regime ($r_s \sim 5$). (ii) KO^+ : The charge-channel KO interaction, which corresponds to $\delta R = 0$ in Eq. (4), agrees well with numerical results in the forward-scattering channel but deviates significantly approaching the Cooper channel. (iii) KO^\pm : The full KO interaction, which further incorporates the spin channel interaction $R_- = \hat{\sigma} \cdot \hat{\sigma}' \left[\frac{f_{\text{XC}}^-}{1 - f_{\text{XC}}^- \Pi_0(q)} - f_{\text{XC}}^- \right]$, performs worse as r_s increases, particularly for antiparallel spins (Fig. 4(d)(f)). The superior performance of KO^+ over KO^\pm suggests that spin interactions are implicitly captured via the exchange component of the charge interaction, without requiring explicit spin-channel terms. (iv) The s-p approximation [18, 19]: It truncates scattering to s- and p-wave channels, which matches our numerical data well, confirming that higher-order partial waves are negligible. However, this approximation is restricted to the Fermi surface and fails to provide a complete effective interaction in other energy scales. In summary, the $s\text{KO}^+$ ansatz resolves the deficiencies of these conventional models, offering a robust effective interaction that is formally applicable beyond the Fermi surface.

We now apply our calculated scattering amplitudes to compute macroscopic transport properties [6, 10, 58], enabling a direct validation of our numerical results against experimental benchmarks. In simple metals, deviations from the Wiedemann–Franz law—which asserts that the electrical resistivity ρ and thermal resistivity W relate to a universal constant L_0 via the equation $\rho/(WT) = L_0$ —are experimentally observed, particularly above the De-

bye temperature [59]. This deviation manifests as an additional thermal resistance with a linear temperature dependence, identified as the electron–electron scattering contribution, W_{ee} [21–24]. However, a precise theoretical description has remained elusive: conventional first-principles DFT typically struggles to capture such dynamical scattering processes, while standard many-body approximations like RPA and the original KO^\pm interaction fail to reproduce the experimental magnitude—yielding significant underestimates and overestimates, respectively (Fig. 1). By contrast, utilizing the full angular dependence of our *ab initio* scattering amplitudes [60], our VDMC calculations achieve excellent agreement with measurements for simple metals (Al, Na, K, Rb), where band mass and core polarization corrections are negligible. Remarkably, this agreement is faithfully reproduced by the computationally efficient sKO^+ ansatz, highlighting its promise for incorporating accurate e-e scattering into first-principles transport calculations of materials. Complementing these macroscopic resistivity results, we also present the quasiparticle scattering rate in the inset of Fig. 1, providing the fundamental timescale governing these transport dynamics [6, 10].

Discussion.—In this work, we present high-precision *ab initio* calculations of the four-point vertex function for the 3D uniform electron gas using our developed VDMC framework. We extract Landau parameters that validate the local density approximation and reveal how the dominant F_0^s parameter drives the system from underscreening toward overscreening as electron density decreases. Our analysis of electron-electron scattering amplitudes on the Fermi surface enables us to establish a simple yet accurate effective model, the sKO^+ ansatz, which is based on the charge KO interaction in LDA with a small s-wave correction. The sufficiency of such short-range corrections parallels recent findings that imperfect screening at short distances necessitates such corrections to capture the physics of the low-density regime. [61]. The excellent agreement between experimental thermal resistivity measurements, our numerical data, and this effective model demonstrates that our results provide a robust foundation for first-principles transport calculations for the electron liquids in simple metals. Looking forward, our methods offer crucial numerical benchmarks for emerging experimental techniques that probe two-particle correlations in materials [15–17]. From the theoretical point of view, the sKO^+ effective interaction will inspire us to construct a better low-energy effective field theory for the fermionic system, consistent with recent insights into the critical role of short-range interactions in low-density metals.

Acknowledgement—K. C. was supported by the National Key Research and Development Program of China, Grant No. 2024YFA1408604, and the National Natural Science Foundation of China under Grants No. 12047503. Z.L, P.H., and Y.D. were supported by the National

Natural Science Foundation of China (under Grant No. 12275263), the Innovation Program for Quantum Science and Technology (under grant No. 2021ZD0301900), the Natural Science Foundation of Fujian Province of China (under Grant No. 2023J02032).

* These two authors contributed equally to this paper.

† bzywang.phys@gmail.com

‡ yjdeng@ustc.edu.cn

§ chenkun@itp.ac.cn

- [1] A. Alexandradinata, N. P. Armitage, A. Baydin, W. Bi, Y. Cao, H. J. Changlani, E. Chertkov, E. H. da Silva Neto, L. Delacretaz, I. E. Baggari, G. M. Ferguson, W. J. Gannon, S. A. A. Ghorashi, B. H. Goodge, O. Goulko, G. Grissonnanche, A. Hallas, I. M. Hayes, Y. He, E. W. Huang, A. Kogar, D. Kumah, J. Y. Lee, A. Legros, F. Mahmood, Y. Maximenko, N. Pellatz, H. Polshyn, T. Sarkar, A. Scheie, K. L. Seyler, Z. Shi, B. Skinner, L. Steinke, K. Thirunavukkuarasu, T. V. Trevisan, M. Vogl, P. A. Volkov, Y. Wang, Y. Wang, D. Wei, K. Wei, S. Yang, X. Zhang, Y.-H. Zhang, L. Zhao, and A. Zong, The future of the correlated electron problem, *SciPost Phys. Comm. Rep.*, 8 (2025).
- [2] E. Dagotto, Correlated electrons in high-temperature superconductors, *Rev. Mod. Phys.* **66**, 763 (1994).
- [3] R. L. Greene, P. R. Mandal, N. R. Poniatowski, and T. Sarkar, The strange metal state of the electron-doped cuprates, *Annual Review of Condensed Matter Physics* **11**, 213 (2020).
- [4] M. Z. Hasan and C. L. Kane, Colloquium: Topological insulators, *Rev. Mod. Phys.* **82**, 3045 (2010).
- [5] P.-F. Loos and P. M. W. Gill, The uniform electron gas, *WIREs Computational Molecular Science* **6**, 410 (2016).
- [6] G. D. Mahan, *Many-particle physics* (Springer Science & Business Media, 2013).
- [7] A. A. Abrikosov, L. P. Gorkov, and I. E. Dzyaloshinski, *Methods of quantum field theory in statistical physics* (Courier Corporation, 2012).
- [8] J. W. Negele, *Quantum many-particle systems* (CRC Press, 2018).
- [9] J. Bardeen, L. N. Cooper, and J. R. Schrieffer, Theory of superconductivity, *Phys. Rev.* **108**, 1175 (1957).
- [10] G. A. Brooker and J. Sykes, Transport properties of a fermi liquid, *Phys. Rev. Lett.* **21**, 279 (1968).
- [11] A. Galler, P. Thunström, P. Gunacker, J. M. Tomczak, and K. Held, Ab initio dynamical vertex approximation, *Phys. Rev. B* **95**, 115107 (2017).
- [12] J. Kaufmann, C. Eckhardt, M. Pickem, M. Kitatani, A. Kauch, and K. Held, Self-consistent ladder dynamical vertex approximation, *Phys. Rev. B* **103**, 035120 (2021).
- [13] B. Cunningham, Many-body vertex effects: Time-dependent interaction kernel with correlated multiexcitons in the bethe-salpeter equation, *Phys. Rev. B* **112**, 115153 (2025).
- [14] J. Zang, M. Medvidović, D. Kiese, D. Di Sante, A. M. Sengupta, and A. J. Millis, Machine learning-based compression of quantum many body physics: Pca and autoencoder representation of the vertex function, *Machine Learning: Science and Technology* **5**, 045076 (2024).
- [15] T. P. Devereaux, M. Claassen, X.-X. Huang, M. Zaletel,

- J. E. Moore, D. Morr, F. Mahmood, P. Abbamonte, and Z.-X. Shen, Angle-resolved pair photoemission theory for correlated electrons, *Phys. Rev. B* **108**, 165134 (2023).
- [16] Y. Su and C. Zhang, Coincidence angle-resolved photoemission spectroscopy: Proposal for detection of two-particle correlations, *Phys. Rev. B* **101**, 205110 (2020).
- [17] E. Fresch, F. V. Camargo, Q. Shen, C. C. Bellora, T. Pullerits, G. S. Engel, G. Cerullo, and E. Collini, Two-dimensional electronic spectroscopy, *Nature Reviews Methods Primers* **3**, 84 (2023).
- [18] K. S. Dy and C. J. Pethick, Transport coefficients of a normal fermi liquid: Application to liquid he^3 , *Phys. Rev.* **185**, 373 (1969).
- [19] A. H. MacDonald and D. J. W. Geldart, Electron-electron scattering and the thermal resistivity of simple metals, *Journal of Physics F: Metal Physics* **10**, 677 (1980).
- [20] C. A. Kukkonen and A. W. Overhauser, Electron-electron interaction in simple metals, *Phys. Rev. B* **20**, 550 (1979).
- [21] J. G. Cook, M. P. V. d. Meer, and M. J. Laubitz, Thermal and electrical conductivities of sodium from 40 to 360 k, *Canadian Journal of Physics* **50**, 1386 (1972), <https://doi.org/10.1139/p72-190>.
- [22] M. J. Laubitz and J. G. Cook, High-temperature thermal resistivity of the polyvalent metals al and pb, *Phys. Rev. B* **7**, 2867 (1973).
- [23] J. G. Cook, Electron-electron scattering in potassium, *Canadian Journal of Physics* **57**, 1216 (1979), <https://doi.org/10.1139/p79-170>.
- [24] C. Uher, Thermal conductivity of metals, in *Thermal Conductivity: Theory, Properties, and Applications*, edited by T. M. Tritt (Springer US, Boston, MA, 2004) pp. 21–91.
- [25] B. Levy, M. Sinvani, and A. J. Greenfield, Sample dependence of the electron-electron contribution to the electrical resistivity of sodium and potassium, *Phys. Rev. Lett.* **43**, 1822 (1979).
- [26] H. van Kempen, J. H. J. M. Ribot, and P. Wyder, The electrical resistivity of potassium at low temperatures, *Journal of Physics F: Metal Physics* **11**, 597 (1981).
- [27] N. R. Shaffer and C. E. Starrett, Model of electron transport in dense plasmas spanning temperature regimes, *Phys. Rev. E* **101**, 053204 (2020).
- [28] J. Lindhard, On the properties of a gas of charged particles, *Kgl. Danske Videnskab. Selskab Mat.-Fys. Medd.* **28** (1954).
- [29] C. A. Kukkonen and J. W. Wilkins, Electron-electron scattering in simple metals, *Phys. Rev. B* **19**, 6075 (1979).
- [30] K. Chen and K. Haule, A combined variational and diagrammatic quantum monte carlo approach to the many-electron problem, *Nature communications* **10**, 1 (2019).
- [31] K. Haule and K. Chen, Single-particle excitations in the uniform electron gas by diagrammatic monte carlo, *Scientific reports* **12**, 2294 (2022).
- [32] N. V. Prokof'ev and B. V. Svistunov, Polaron problem by diagrammatic quantum monte carlo, *Phys. Rev. Lett.* **81**, 2514 (1998).
- [33] N. Prokof'ev and B. Svistunov, Fermi-polaron problem: Diagrammatic monte carlo method for divergent sign-alternating series, *Phys. Rev. B* **77**, 020408(R) (2008).
- [34] E. Kozik, M. Ferrero, and A. Georges, Nonexistence of the luttinger-ward functional and misleading convergence of skeleton diagrammatic series for hubbard-like models, *Phys. Rev. Lett.* **114**, 156402 (2015).
- [35] R. Rossi, Determinant diagrammatic monte carlo algorithm in the thermodynamic limit, *Phys. Rev. Lett.* **119**, 045701 (2017).
- [36] N. Prokof'ev and B. Svistunov, Bold diagrammatic monte carlo technique: When the sign problem is welcome, *Phys. Rev. Lett.* **99**, 250201 (2007).
- [37] R. Rossi, T. Ohgoe, K. Van Houcke, and F. Werner, Resummation of diagrammatic series with zero convergence radius for strongly correlated fermions, *Phys. Rev. Lett.* **121**, 130405 (2018).
- [38] K. Van Houcke, F. Werner, E. Kozik, N. V. Prokof'ev, B. V. Svistunov, M. Ku, A. Sommer, L. Cheuk, A. Schirrotzek, and M. Zwierlein, Feynman diagrams versus fermi-gas feynman emulator, *Nature Physics* **8**, 366 (2012).
- [39] S. Brolli, C. Barbieri, and E. Vigezzi, Diagrammatic monte carlo for finite systems at zero temperature, *Phys. Rev. Lett.* **134**, 182502 (2025).
- [40] Y. Wang and K. Haule, Variational diagrammatic monte carlo built on dynamical mean-field theory, *Phys. Rev. Lett.* **135**, 176501 (2025).
- [41] P. Hou, T. Wang, D. Cerkoney, X. Cai, Z. Li, Y. Deng, L. Wang, and K. Chen, An ai-powered technology stack for solving many-electron field theory (2025), [arXiv:2403.18840 \[hep-th\]](https://arxiv.org/abs/2403.18840).
- [42] Z. Li, P. Hou, Y. Deng, and K. Chen, Matsubara-frequency-resolved spin exchange-correlation kernel for the three-dimensional uniform electron gas, *Phys. Rev. B* **111**, 155132 (2025).
- [43] P.-C. Hou, B.-Z. Wang, K. Haule, Y. Deng, and K. Chen, Exchange-correlation effect in the charge response of a warm dense electron gas, *Phys. Rev. B* **106**, L081126 (2022).
- [44] K. Chen, Partial renormalization of quasiparticle interactions (2024), [arXiv:2404.15844 \[cond-mat.str-el\]](https://arxiv.org/abs/2404.15844).
- [45] Y. Takada, Quasiparticle properties of the electron gas at metallic densities in the effective-potential expansion method, *Phys. Rev. B* **43**, 5979 (1991).
- [46] K. Matsuda, K. Tamura, and M. Inui, Instability of the electron gas in an expanding metal, *Phys. Rev. Lett.* **98**, 096401 (2007).
- [47] K. Takayanagi and E. Lipparini, Ghost plasmon and negative dielectric function, *Phys. Rev. B* **56**, 4872 (1997).
- [48] J. P. Perdew and Y. Wang, Accurate and simple analytic representation of the electron-gas correlation energy, *Phys. Rev. B* **45**, 13244 (1992).
- [49] V. Silin, Theory of a degenerate electron liquid, *Sov. Phys. JETP-USSR* **6**, 387 (1958).
- [50] V. Silin, On the theory of the anomalous skin effect in metals, *Soviet Physics JETP* **6**, 33 (1958).
- [51] H. Maebashi and Y. Takada, Pseudo-quantum criticality in electron liquids exhibited in expanded alkali metals (2007), [arXiv:0706.4001 \[cond-mat.other\]](https://arxiv.org/abs/0706.4001).
- [52] A further discussion of this crossover phenomenon will be discussed in Sec. IV in the supplemental material with our numerical results of the density response function and the ion-ion interaction.
- [53] Y. Takada, Low-energy peak in the one-particle spectral function of the electron gas at metallic densities, *Phys. Rev. B* **110**, 085132 (2024).
- [54] M. Holzmann, B. Bernu, V. Olevano, R. M. Martin, and D. M. Ceperley, Renormalization factor and effective

- mass of the two-dimensional electron gas, Phys. Rev. B **79**, 041308 (2009).
- [55] X. Cai, T. Wang, N. V. Prokof'ev, B. V. Svistunov, and K. Chen, Superconductivity in the uniform electron gas: Irrelevance of the kohn-luttinger mechanism, Phys. Rev. B **106**, L220502 (2022).
- [56] H.-W. Hammer and R. Furnstahl, Effective field theory for dilute fermi systems, Nuclear Physics A **678**, 277 (2000).
- [57] C. Wellenhofer, C. Drischler, and A. Schwenk, Dilute fermi gas at fourth order in effective field theory, Physics Letters B **802**, 135247 (2020).
- [58] H. H. Jensen, H. Smith, and J. W. Wilkins, Upper and lower bounds on transport coefficients arising from a linearized boltzmann equation, Phys. Rev. **185**, 323 (1969).
- [59] C. Kittel and P. McEuen, *Introduction to solid state physics* (John Wiley & Sons, 2018).
- [60] See Sec. SVI in the supplemental material.
- [61] J. Koskelo, L. Reining, and M. Gatti, Short-range excitonic phenomena in low-density metals, Phys. Rev. Lett. **134**, 046402 (2025).

Supplemental Material

SI. VARIATIONAL DIAGRAMMATIC MONTE CARLO METHOD AND CONVERGENCE ANALYSIS

In this section, we provide the theoretical foundation and technical details of the Variational Diagrammatic Monte Carlo (VDMC) framework employed in the main text.

Our investigation is grounded in the standard Hamiltonian for the Uniform Electron Gas (UEG). In the second-quantization formalism, the system consists of interacting quasi-electrons and is described by the Hamiltonian:

$$H = \sum_{\mathbf{k}\sigma} (\mathbf{k}^2 - \mu) \psi_{\mathbf{k}\sigma}^\dagger \psi_{\mathbf{k}\sigma} + \frac{1}{2} \sum_{\substack{\mathbf{q} \neq 0 \\ \mathbf{k}\mathbf{k}'\sigma\sigma'}} v_q \psi_{\mathbf{k}+\mathbf{q}\sigma}^\dagger \psi_{\mathbf{k}'-\mathbf{q}\sigma'}^\dagger \psi_{\mathbf{k}'\sigma'} \psi_{\mathbf{k}\sigma}, \quad (\text{S1})$$

where $\psi_{\mathbf{k}\sigma}$ and $\psi_{\mathbf{k}\sigma}^\dagger$ are the annihilation and creation operators for an electron with momentum \mathbf{k} and spin σ , and μ denotes the chemical potential determined by the density parameter r_s . A significant challenge in addressing the many-body problem of this Hamiltonian arises from the long-range nature of the bare Coulomb interaction, $v_q = 8\pi/q^2$. Standard diagrammatic expansions suffer from infrared divergences due to this long-range interaction [1]. The VDMC method resolves this by expanding around a screened Yukawa interaction [2–6], $v_q^\lambda = 8\pi/(q^2 + \lambda)$, where λ is a variational parameter. To maintain the original physics, we introduce a polarization counterterm $-\lambda/8\pi$ and chemical potential counterterms. These corrections effectively cancel large particle-hole fluctuations and ensure a fixed particle density at every order. Specifically, the parameter λ is subject to iterative optimization to ensure convergence.

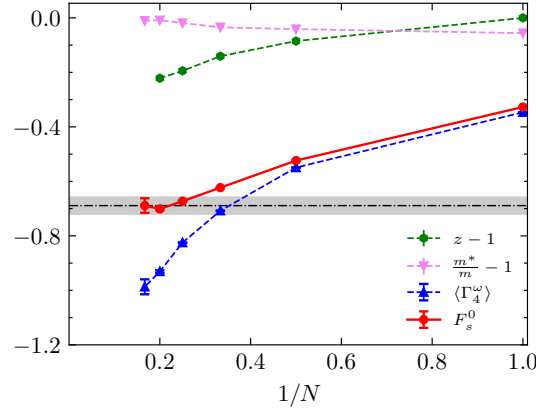


FIG. S1: Convergence of the Landau parameter F_s^0 and its constituent parts—the quasiparticle weight $(z - 1)$, the effective mass $((m^*/m) - 1)$, and the four-point vertex $(\langle \Gamma_4^\omega \rangle)$ —as a function of inverse perturbation order $1/N$ for the uniform electron gas at $r_s = 4.0$. The combined quantity F_s^0 converges significantly faster than its individual components.

In this work, we developed an efficient technique to achieve rapid convergence in our calculations. We illustrate this method using the Landau parameter F_0^s , a key quantity discussed in the main text. This parameter relates to the quasiparticle weight z , the effective mass ratio m^*/m , and the angular average of the four-point vertex function $\langle \Gamma_4^\omega \rangle$. As defined in the main text, the vertex function takes the form $\Gamma_4^\omega = \lim_{\mathbf{q} \rightarrow 0} [\Gamma_4^{\sigma\sigma'}(\mathbf{k}_1\omega_{-1}, \mathbf{k}_2\omega_0; \mathbf{k}_1 + \mathbf{q}\omega_0) - v_q]$. The Landau parameter is then given by the relation $F_0^s = z^2(m^*/m)\langle \Gamma_4^\omega \rangle$, where $\langle \dots \rangle$ denotes the average over the angle between \mathbf{k}_1 and \mathbf{k}_2 on the Fermi surface. We compute the perturbative expansions of these constituent quantities in powers of a formal parameter ξ using the same variational screening parameter λ :

$$\begin{aligned} z &= 1 + z_1\xi + z_2\xi^2 + \dots, \\ m^*/m &= 1 + m_1\xi + m_2\xi^2 + \dots, \\ \langle \Gamma_4^\omega \rangle &= \gamma_1\xi + \gamma_2\xi^2 + \dots, \end{aligned} \quad (\text{S2})$$

where z is derived from the numerical calculation of the self energy diagram and m^*/m is derived from the calculation of F_1^s , specifically, $m^*/m = 1/(1 - z^2\langle \Gamma_4^\omega \cos\theta \rangle)$. Substituting these into the expression for the Landau parameter

yields a series expansion $F_0^s = F^{(1)}\xi + F^{(2)}\xi^2 + \dots$, where the coefficients are determined order by order. Specifically, the first and second-order coefficients are given by:

$$F^{(1)} = \gamma_1, \quad (\text{S3})$$

$$F^{(2)} = \gamma_2 + (2z_1\gamma_1 + m_1\gamma_1). \quad (\text{S4})$$

The rapid convergence observed in our results stems from a systematic cancellation between competing physical processes in this expansion. For instance, in the second-order contribution $F^{(2)}$, the direct correction to the vertex function γ_2 is typically negative, whereas the term arising from the renormalization of the quasiparticle weight and effective mass $(2z_1\gamma_1 + m_1\gamma_1)$ is typically positive. These dominant terms partially cancel each other, significantly reducing the magnitude of $F^{(2)}$ and effectively accelerating the overall convergence as shown in Fig. S1.

SII. NUMERICAL RESULTS OF THE LANDAU PARAMETERS

In this section, we present the precise numerical values of the Landau parameters derived from our VDMC calculations, which are summarized in Table S1.

As discussed in the main text, the symmetric Landau parameter F_0^s plays a pivotal role in characterizing the density-driven crossover from underscreening to overscreening. However, compared to the higher angular momentum components and the antisymmetric channels, F_0^s exhibits relatively slower convergence, particularly in the strong coupling regime. To ensure the numerical stability and robustness of this critical quantity, we extended our diagrammatic expansion to the sixth order for the calculation of F_0^s . For the other Landau parameters ($F_{l>0}^s$ and F_l^a), a truncation at the fifth order was found to be sufficient in our discussion.

r_s	1.0	2.0	3.0	4.0	5.0	6.0
F_0^s	-0.210(2)	-0.367(6)	-0.52(2)	-0.69(3)	-0.84(4)	-1.08(10)
F_1^s	-0.049(3)	-0.047(4)	-0.040(3)	-0.030(4)	-0.024(3)	-0.015(4)
F_2^s	-0.028(1)	-0.030(3)	-0.030(2)	-0.029(2)	-0.030(4)	-0.031(5)
F_0^a	-0.175(1)	-0.261(5)	-0.320(9)	-0.362(5)	-0.400(5)	-0.43(2)
F_1^a	-0.066 4(4)	-0.088(5)	-0.103(3)	-0.115(7)	-0.124(5)	-0.135(6)
F_2^a	-0.019 6(6)	-0.012 4(6)	-0.006 0(4)	-0.001 3(4)	0.001(4)	0.002(4)

TABLE S1: Numerical results of the Landau parameters.

SIII. MICROSCOPIC INSIGHTS FOR THE RELATION BETWEEN THE FERMI LIQUID THEORY AND LINEAR RESPONSE THEORY

In this section, we provide a detailed microscopic derivation of the density-density correlation function and the effective electron-electron interaction. By bridging the diagrammatic definition of the response function with microscopic theory, we clarify the physical origin of the relation between the Landau parameter and the exchange-correlation kernel (Eq. (3) in the main text) discovered by our numerical results.

We begin with the density-density correlation function $\chi(q)$ in the imaginary-time formalism:

$$\chi(q) = \int_0^\beta \langle \mathcal{T} \hat{\rho}(\mathbf{q}, \tau) \hat{\rho}(\mathbf{q}, 0) \rangle e^{i\omega_n \tau} d\tau, \quad (\text{S5})$$

where \mathcal{T} is the time-ordering operator, the density operator $\hat{\rho}(\mathbf{q}, \tau) = \sum_{\mathbf{p}, \sigma} \hat{c}_{\mathbf{p}+\mathbf{q}, \sigma}^\dagger(\tau) \hat{c}_{\mathbf{p}, \sigma}(\tau)$ and $q \equiv (i\omega_n, \mathbf{q})$ is the Matsubara-frequency/momentum vector. Through the Eliashberg equation [7] as shown in Fig. S2, $\chi(q)$ is related to the four-point vertex function $\Gamma^4(p, p', k)$ and the quasiparticle Green's function $G(p)$ by the equation

$$\chi(q) = \sum_{p\sigma} G_\sigma(p+q)G_\sigma(p) + \sum_{p\sigma, p'\sigma'} G_\sigma(p+q)G_\sigma(p)\Gamma_{\sigma\sigma'}^4(p, p', q)G_{\sigma'}(p')G_{\sigma'}(p'-q), \quad (\text{S6})$$

Near the Fermi surface, the Green's function takes the form $G_\sigma(p) \approx \frac{z}{i\epsilon_n - v_F(|\mathbf{p}| - k_F)}$, where v_F is the Fermi velocity and z is the quasiparticle renormalization factor.

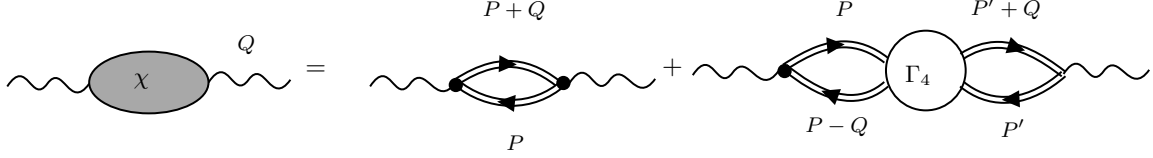


FIG. S2: Feynman diagrams for the Eliashberg equation.

For small momentum and energy transfer ($q \rightarrow 0$), the product of Green's functions $g_\sigma(p, q) \equiv G_\sigma(p)G_\sigma(p+q)$ exhibits a singularity arising from the Fermi surface poles. It can be decomposed into a singular part Π and a regular part ϕ :

$$g_\sigma(p, q) \equiv G_\sigma(p)G_\sigma(p+q) \sim \Pi(p, q)\delta(i\epsilon_n)\delta(|\mathbf{p}| - k_F) + \phi(p), \quad (\text{S7})$$

The first term captures the particle-hole excitations restricted to the Fermi surface, while $\phi(p)$ represents contributions from high-energy excitations. To simplify the derivation, we adopt a matrix notation where multiplication implies summation over momentum p and spin σ . The correlation function can be compactly written as:

$$\chi(q) = \text{Tr}[g(1 + \Gamma_4 g)]. \quad (\text{S8})$$

We introduce the quasiparticle irreducible vertex function Γ^ω , defined in the limit where $q \rightarrow 0$ with $|\mathbf{q}|/\omega_n \rightarrow 0$. This quantity is related to the full vertex Γ_4 through a Dyson-like equation involving the singular part Π :

$$\Gamma_4 = \Gamma^\omega + \Gamma^\omega \Pi \Gamma_4. \quad (\text{S9})$$

Crucially, in Landau Fermi liquid theory [8], this irreducible vertex Γ^ω is directly related to the Landau quasiparticle interaction $f_{\sigma\sigma'}(\theta)$ on the Fermi surface:

$$f_{\sigma\sigma'}(\theta) = z^2 \Gamma_{\sigma\sigma'}^\omega(\mathbf{p}_F, \mathbf{p}'_F). \quad (\text{S10})$$

To solve for the response function, we employ a matrix identity introduced in Ref. [9]: for matrices satisfying $f = f_1 + f_2$ and $S = S_0 + S_0 f_2 S$, one can derive:

$$f(1 + Sf) = f_1(1 + S_0 f_1) + (1 + f_1 S_0) f_2 (1 - S_0 f_2)^{-1} (1 + S_0 f_1). \quad (\text{S11})$$

Identifying $f \rightarrow g$, $S \rightarrow \Gamma_4$, and using the decomposition $g = \phi + \Pi$, we utilize the Ward identity relation $1 + \sum \phi \Gamma^\omega = 1/z$ [10] to simplify the resulting expression. This leads to:

$$\chi(q) = \Phi + \frac{1}{z^2} \text{Tr}[\Pi(1 - \Gamma^\omega \Pi)^{-1}], \quad (\text{S12})$$

where $\Phi = \text{Tr}[\phi(1 + \phi \Gamma^\omega)]$. It can be further shown that the regular contribution Φ vanishes ($\Phi = 0$). Thus, the response function is determined solely by the Fermi surface contributions:

$$\chi(q) = \frac{1}{z^2} \sum_{\theta, \sigma} \frac{\Pi(\theta)}{1 - \sum_{\theta', \sigma'} \Gamma_{\sigma\sigma'}^\omega(\theta, \theta') \Pi(\theta')}, \quad (\text{S13})$$

where θ and θ' denote the angles between the transfer momentum \mathbf{q} and the momenta of the incoming quasiparticles \mathbf{p} and \mathbf{p}' , respectively.

Substituting the Landau parameter relation $\Gamma^\omega = z^{-2} f$, the equation becomes:

$$\chi(q) = \frac{1}{z^2} \sum_{\theta, \sigma} \frac{\Pi(\theta)}{1 - \sum_{\theta', \sigma'} z^{-2} f_{\sigma\sigma'}(\theta, \theta') \Pi(\theta')}. \quad (\text{S14})$$

In the static limit $q = (0, \mathbf{q})$, the term $\sum \Pi(\theta)$ corresponds to the renormalized Lindhard function: $\sum \Pi = z^2(m^*/m)\Pi_0(q)$.

Supported by the numerical results shown in Figs. 2 and 3 in the main text, the angle dependence of the Landau quasiparticle interaction in the uniform electron gas is sufficiently weak that the interaction is dominated by the zeroth-order term ($f_0^s \gg f_l^s$ for $l \geq 1$). We can therefore approximate it using the zeroth-order Landau parameter

$f_0^s = F_0^s/N_F^*$, where N_F^* denotes the quasiparticle density of states. By explicitly including the long-range Coulomb interaction $v_q = 4\pi e^2/q^2$ —which enters the singlet channel as $v_q + f_0^s$ in Landau-Silin theory [11, 12]—the response function simplifies to:

$$\chi(q) \approx \frac{\frac{m^*}{m}\Pi_0(q)}{1 - \frac{m^*}{m}(v_q + f_0^s)\Pi_0(q)}. \quad (\text{S15})$$

This expression takes a form similar to the response function defined by the exchange-correlation kernel f_{xc} , written as $\chi = \Pi_0(q)/[1 - (v_q + f_{xc}(q))\Pi_0(q)]$. Furthermore, our numerical results indicate that the effective mass ratio m^*/m approaches unity in the metallic regime. Based on this, we validate the local density approximation and the relationship presented in Eq. (3) of the main text:

$$f_{xc}(q) \approx f_{xc}(q=0) \approx \frac{F_0^s}{N_F^*}, \quad (\text{S16})$$

for the metallic gas.

By revisiting Eq. (S9), we can derive that

$$\Gamma_4 = \Gamma_4^\omega (1 - \Gamma_4^\omega \Pi)^{-1}, \quad (\text{S17})$$

which encodes the singular part of the two-electron correlation structure as $\omega/q \rightarrow 0$. Then, we can obtain the form of the effective electron-electron interaction within the local density approximation and Landau-Silin theory as

$$R(q) \sim \frac{v_q + f_0^s}{1 - \frac{m^*}{m}(v_q + f_0^s)\Pi_0(q)}. \quad (\text{S18})$$

To describe the behavior of the effective interaction in the finite- q area, one can add a regular term to ensure that the effective interaction vanishes as $q \rightarrow \infty$. Therefore, we have

$$R(q) = \frac{v_q + f_0^s}{1 - \frac{m^*}{m}(v_q + f_0^s)\Pi_0(q)} - f_0^s. \quad (\text{S19})$$

This effective interaction also share the same structure of the charge-based Kukkonen-Overhauser interaction derived from the linear response theory [13].

SIV. CROSSOVER OF THE COULOMB SCREENING EFFECT

In this section, we provide further details on the density-driven crossover of the Coulomb screening effect discussed in the main text. To visualize this phenomenon, we employed the VDMC method to calculate the static density-density correlation function, $\chi(q)$, and the effective test charge-test charge interaction $W_{tt}(q)$, which relates to the ion-ion interaction for metals, as shown in Fig. S3. In the linear response formalism, $W_{tt}(q)$ is expressed in terms of the bare Coulomb potential v_q , the non-interacting Lindhard polarizability $\Pi_0(q)$, and the static exchange-correlation kernel $f_{xc}(q)$ as:

$$W_{tt}(q) = \frac{v_q[1 - f_{xc}(q)\Pi_0(q)]}{1 - [v_q + f_{xc}(q)]\Pi_0(q)}.$$

To disentangle many-body correlations from the Coulomb singularity, we analyzed the normalized response function $\chi(q)v_q/\chi_0(q)$. As shown in Fig. S3a, the microscopic VDMC results exhibit remarkable agreement with benchmark Diffusion Monte Carlo (DMC) data [14] and theoretical predictions using a static kernel $f_{xc}(q) = f_{xc}(0)$ (which is represented by the dash lines). This concordance confirms that the local approximation effectively captures the essential screening physics in the small- q regime.

The numerical results clearly manifest a physical crossover in the density regime $5 < r_s < 6$, consistent with the compressibility divergence ($F_0^s \rightarrow -1$). For metallic densities ($r_s < r_s^c$), the system resides in the conventional underscreening regime, characterized by positive static compressibility and a purely repulsive effective interaction. Conversely, as the density decreases ($r_s > r_s^c$), an overscreening phase emerges where the static compressibility and dielectric function become negative in the long-wavelength limit. Physically, this induces a counter-intuitive attractive interaction between like-charged test particles at large distances, as evidenced by the negative tail in $W_{tt}(q)$ (Fig. S3b), while the interaction remains repulsive at short ranges. Additionally, Figure S3a suggests that this crossover may be related to a stable RG fixed point, as $\chi_0 N_F / \chi_q v_q$ approaches 1 as $q \rightarrow 0$ for any r_s .

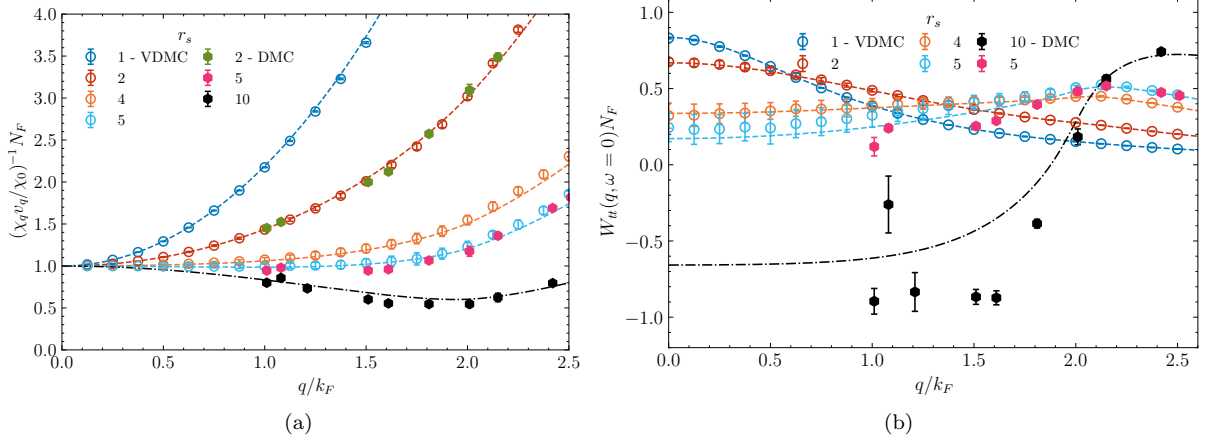


FIG. S3: (a) The inverse normalized density-density response function, $(\chi_q v_q / \chi_0)^{-1} N_F$, calculated for various r_s . The symbols represent data from Variational Diagrammatic Monte Carlo (VDMC, open circles) and Diffusion Monte Carlo (DMC, filled symbols) [14]. The dashed lines correspond to the theoretical prediction using the LDA approximation. (b) The effective test charge-test charge interaction $W_{tt}(q, \omega = 0)$ normalized by the Fermi density of states N_F . The transition from positive to negative values at small momenta signals the onset of the overscreening phase. The excellent agreement between the VDMC/DMC data and the LDA-based curves confirms that the effectiveness of the local density approximation.

SV. RESULTS OF THE GENERAL POLYNOMIAL EXPANSION

In this section, we detail the procedure for deriving the residual part of the scattering amplitude that extends beyond the charge-only Kukkonen-Overhauser (KO^+) ansatz. To rigorously compare theoretical ansatzes with the numerical scattering amplitudes $A^{\sigma\sigma'}(\theta, \phi)$ computed via VDMC, we first establish the general mapping between effective interaction potentials $R(\mathbf{q})$ and the observable scattering amplitudes. This construction relies on the specific spin configuration and the requirements imposed by the Pauli exclusion principle.

For fermions with parallel spins ($\uparrow\uparrow$), the total wavefunction must be antisymmetric with respect to particle exchange. Consequently, the scattering amplitude is constructed as the difference between the direct interaction term, with momentum transfer $\mathbf{q} = \mathbf{k}_1 - \mathbf{k}_3$, and the exchange interaction term, with momentum transfer $\mathbf{q}' = \mathbf{k}_1 - \mathbf{k}_4$. The resulting amplitude takes the form:

$$a^{\uparrow\uparrow}(\theta, \phi) = R^{\uparrow\uparrow}(\mathbf{k}_1 - \mathbf{k}_3) - R^{\uparrow\uparrow}(\mathbf{k}_1 - \mathbf{k}_4). \quad (\text{S20})$$

In contrast, for the antiparallel spin channel ($\uparrow\downarrow$), the particles are distinguishable, and in the standard formulation of charge-channel models such as the KO^+ and our proposed sKO^+ ansatz, only the direct scattering process contributes to the amplitude:

$$a^{\uparrow\downarrow}(\theta, \phi) = R^{\uparrow\downarrow}(\mathbf{k}_1 - \mathbf{k}_3). \quad (\text{S21})$$

It is worth noting that for the full Kukkonen-Overhauser interaction (KO^\pm), which explicitly incorporates a transverse spin-exchange interaction R_{KO^-} mediated by spin fluctuations, the antiparallel amplitude acquires an additional contribution. In that specific case, the amplitude is modified to $a_{\text{KO}^\pm}^{\uparrow\downarrow}(\theta, \phi) = R^{\uparrow\downarrow}(\mathbf{k}_1 - \mathbf{k}_3) - 2R_{\text{KO}^-}(\mathbf{k}_1 - \mathbf{k}_4)$.

To systematically quantify the correlations terms from the KO^+ , we analyze the residual scattering amplitude, defined as $\delta A^{\sigma\sigma'}(\theta, \phi) = A_{\text{VDMC}}^{\sigma\sigma'}(\theta, \phi) - A_{\text{KO}^+}^{\sigma\sigma'}(\theta, \phi)$. We perform a general polynomial expansion of this residual part using a set of basis functions $X_{lk}(\theta, \phi)$ that are orthogonal on the Fermi surface [15]:

$$\delta A^{\sigma\sigma'}(\theta, \phi) = \sum_{k=0}^{\infty} \sum_{l=0}^k \delta A_{lk}^{\sigma\sigma'} X_{lk}(\theta, \phi). \quad (\text{S22})$$

The basis functions are constructed from Legendre polynomials $P_l(x)$ and Jacobi polynomials $P_n^{(a,b)}(x)$ as $X_{lk}(\theta, \phi) = (-1)^l (k+1)^{\frac{1}{2}} (2l+1)^{\frac{1}{2}} \sin^{2l}(\theta/2) P_l(\cos \phi) P_{k-l}^{(2l+1,0)}(\cos \theta)$.

As illustrated in Fig. S4, the resulting expansion coefficients $\delta A_{lk}^{\sigma\sigma'}$ reveal a clear physical distinction between the spin channels. For parallel spins, the coefficients are negligible, confirming that the KO^+ ansatz provides a sufficient description of the interaction. However, for antiparallel spins, the residual is significantly non-zero and is clearly dominated by the isotropic $(l, k) = (0, 0)$ and $(0, 1)$ components. This observation justifies parameterizing the residual effective interaction, $\delta R^{\uparrow\downarrow}$, as a simple s-wave contact interaction, analogous to effective field theories for dilute Fermi systems [16, 17]:

$$\delta R^{\uparrow\downarrow}(\mathbf{k}_1, \mathbf{k}_2; \mathbf{k}_3, \mathbf{k}_4) = C_0 + C_2 \frac{(\mathbf{k}_1 - \mathbf{k}_2)^2 + (\mathbf{k}_3 - \mathbf{k}_4)^2}{2}, \quad (\text{S23})$$

with higher order p-wave correction $C_2'(\mathbf{k}_1 - \mathbf{k}_2) \cdot (\mathbf{k}_3 - \mathbf{k}_4)$ negligible as shown in Fig. S4. In this expression, the leading-order constant C_0 , which is proportional to the s-wave scattering length, is determined by the dominant $\delta A_{00}^{\uparrow\downarrow}$ component. The next-to-leading-order constant C_2 , related to the s-wave effective range, is fixed by the sub-dominant term $\delta A_{01}^{\uparrow\downarrow}$. This derived correction term δR with its relevant parameters shown in the inset of Fig. S4 constitutes the basis of the sKO^+ ansatz employed in the main text.

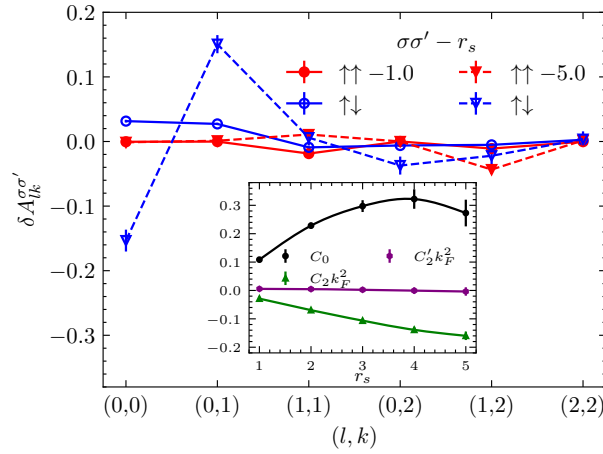


FIG. S4: General polynomial expansion [15] of the residual part of the scattering amplitude. Inset: Parametrization of the effective field action describing the electron-electron correlation beyond the KO^+ ansatz. Here, C_0 relates to the s-wave scattering length, C_2 relates to the s-wave effective range, C_2' relates to a higher order p-wave correction which is negligible. It shows the residual part can be described by a s-wave scattering process.

SVI. TRANSPORT PROPERTIES DERIVED THROUGH THE SCATTERING AMPLITUDE

As is mentioned in the main text, the knowledge of the electron-electron scattering amplitude $a_{\sigma\sigma'}(\theta, \phi)$ will help us derive the contribution of the electron-electron scattering to several transport properties, for example, the electron-electron scattering rate $1/\tau$ and the thermal resistivity W_{ee} . Specifically, they are derived from the following formulas [18–20],

$$W_{ee} = \frac{3(m^*)^4 T}{8\pi^2 \hbar^6 k_F^3 H(\lambda)} \left\langle \frac{\omega(\theta, \phi)(1 - \cos \theta)}{\cos \frac{\theta}{2}} \right\rangle, \quad (\text{S24})$$

$$B_{ee} = \frac{3(m^*)^4}{8\pi^2 \hbar^6 k_F^3 H(\lambda)} \left\langle \frac{\omega(\theta, \phi)(1 - \cos \theta)}{\cos \frac{\theta}{2}} \right\rangle \quad (\text{S25})$$

$$\frac{1}{\tau} = \frac{(m^*)^3}{16\pi^2 \hbar^6} (k_B T)^2 \left\langle \frac{\omega(\theta, \phi)}{\cos \frac{\theta}{2}} \right\rangle, \quad (\text{S26})$$

where

$$H(\lambda) = \frac{3-\lambda}{4} \sum_{n=0}^{\infty} \frac{4n+5}{(n+1)(2n+3)[(n+1)(2n+3)-\lambda]}, \quad (\text{S27})$$

$$\lambda = \frac{\langle \omega(\theta, \phi)(1+2\cos\theta)/\cos\frac{\theta}{2} \rangle}{\langle \omega(\theta, \phi)/\cos\frac{\theta}{2} \rangle}, \quad (\text{S28})$$

$$\omega(\theta, \phi) = \frac{2\pi}{\hbar} \left[\frac{1}{2} |a_{\uparrow\downarrow}(\theta, \phi)|^2 + \frac{1}{4} |a_{\uparrow\uparrow}(\theta, \phi)|^2 \right]. \quad (\text{S29})$$

with $\langle \dots \rangle = \frac{1}{4\pi} \int_0^{2\pi} d\phi \int_0^\pi d\theta \sin\theta$ denotes the average over the solid angle. As mentioned in the main text, the s-p approximation proposed by Dy and Pethick [21, 22], which approximate the electron-electron scattering amplitude within the contribution of s-wave and p-wave scattering, which also shows good agreement with the experimental results. Specifically, the scattering amplitude can be written as

$$a_{\uparrow\uparrow}^{sp}(\theta, \phi) = \frac{\cos\phi}{N_F^*} [(A_0^s + A_0^a) + 3(A_1^s + A_1^a) \cos\theta], \quad (\text{S30})$$

$$a_{\uparrow\downarrow}^{sp}(\theta, \phi) = \frac{\cos\phi}{2N_F^*} [(A_0^s + A_0^a) + 3(A_1^s + A_1^a) \cos\theta] + A_0^s - 3A_0^a + 3(A_1^s - 3A_1^a) \cos\theta \quad (\text{S31})$$

where $A_l^{s,a} = \frac{F_l^{s,a}}{1+F_l^{s,a}}$ can be derived from the Landau parameter.

-
- [1] K. Van Houcke, I. S. Tupitsyn, and N. V. Prokof'ev, Diagrammatic monte carlo and gw approximation for jellium and hydrogen chain, in *Handbook of Materials Modeling*, edited by W. Andreoni and S. Yip (Springer International Publishing, Cham, 2020) pp. 435–452.
 - [2] K. Chen and K. Haule, Nature communications **10**, 1 (2019).
 - [3] K. Haule and K. Chen, Scientific reports **12**, 2294 (2022).
 - [4] P. Hou, T. Wang, D. Cerkoney, X. Cai, Z. Li, Y. Deng, L. Wang, and K. Chen, An ai-powered technology stack for solving many-electron field theory (2025), arXiv:2403.18840 [hep-th].
 - [5] R. Rossi, F. Werner, N. Prokof'ev, and B. Svistunov, Phys. Rev. B **93**, 161102 (2016).
 - [6] M. E. Peskin, *An introduction to quantum field theory* (CRC press, 2018).
 - [7] G. Eliashberg, Sov. Phys. JETP **14**, 886 (1962).
 - [8] L. Landau, Sov. Phys. JETP **8**, 70 (1959).
 - [9] A. J. Leggett, Phys. Rev. **140**, A1869 (1965).
 - [10] A. A. Abrikosov, L. P. Gorkov, and I. E. Dzyaloshinski, *Methods of quantum field theory in statistical physics* (Courier Corporation, 2012).
 - [11] V. Silin, Sov. Phys. JETP-USSR **6**, 387 (1958).
 - [12] V. Silin, Soviet Physics JETP **6**, 33 (1958).
 - [13] C. A. Kukkonen and A. W. Overhauser, Phys. Rev. B **20**, 550 (1979).
 - [14] S. Moroni, D. M. Ceperley, and G. Senatore, Phys. Rev. Lett. **75**, 689 (1995).
 - [15] M. Pfizner, Journal of low temperature physics **61**, 141 (1985).
 - [16] H.-W. Hammer and R. Furnstahl, Nuclear Physics A **678**, 277 (2000).
 - [17] C. Wellenhofer, C. Drischler, and A. Schwenk, Physics Letters B **802**, 135247 (2020).
 - [18] G. D. Mahan, *Many-particle physics* (Springer Science & Business Media, 2013).
 - [19] H. H. Jensen, H. Smith, and J. W. Wilkins, Phys. Rev. **185**, 323 (1969).
 - [20] G. A. Brooker and J. Sykes, Phys. Rev. Lett. **21**, 279 (1968).
 - [21] K. S. Dy and C. J. Pethick, Phys. Rev. **185**, 373 (1969).
 - [22] A. H. MacDonald and D. J. W. Geldart, Journal of Physics F: Metal Physics **10**, 677 (1980).